AD-A084 223 AERONAUTICAL SYSTEMS DIV WRIGHT-PATTERSON AFB OH DEPU--ETC F/G 17/9
TACTICAL TARGET ACQUISITION MODEL (TATAC). VOLUME I. ANALYSTS' --ETC(U)
DEC 77 S BAILY
UNCLASSIFIED ASD/XR-TR-79-5029-VOL-1 NL

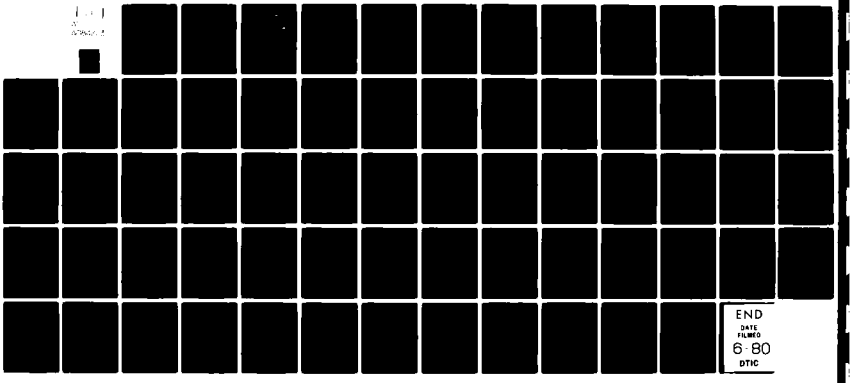

END
DATE FILMED
6-80
DTIC

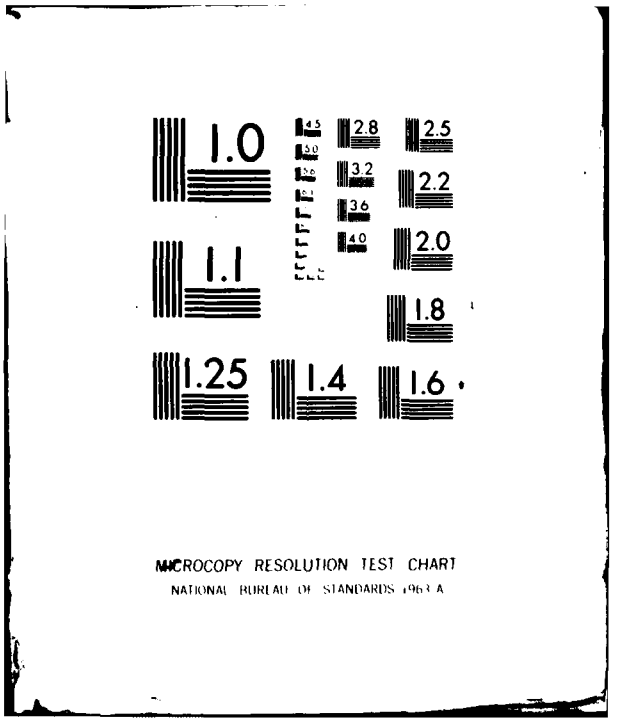
1.0
1.1
1.25
1.4
1.6
1.8
2.0
2.2
2.5
2.8
3.2
3.6
4.0
4.5
5.0
MICROCOPY RESOLUTION TEST CHART
NATIONAL BUREAU OF STANDARDS 1963 A

ASD/XR-TR-79-5029

LEVEL II

Ops/Analysis

Directorate Of Operations Research

ADA084223

TACTICAL TARGET ACQUISITION MODEL (TATAC)

VOLUME I

ANALYSTS' MANUAL

DECEMBER 1977

PREPARED FOR ASD BY

LULEJIAN AND ASSOCIATES, INC.

DEPUTY FOR DEVELOPMENT PLANNING
AERONAUTICAL SYSTEMS DIVISION
WRIGHT-PATTERSON AIR FORCE BASE, OHIO

NOTICES

When Government drawings, specifications, or other data are used for any purpose other than in connection with a definitely related Government procurement operation, the United States Government thereby incurs no responsibility nor any obligation whatsoever; and the fact that the Government may have formulated, furnished or in any way supplied the said drawings, specifications, or other data is not to be regarded by implication or otherwise as in any manner licensing the holder or any other person or corporation, or conveying any rights to permission to manufacture, use, or sell any patented invention that may in any way be related thereto.

Copies of this report should not be returned to the Aeronautical Systems Division unless return is required by security considerations, contractual obligations, or notice on a specific document.

Publication of this technical report does not constitute Air Force approval of the report's findings or conclusions. It is published only for the exchange and stimulation of ideas.

This technical report has been reviewed and is approved for publication.

S. A. TREMAINE
Deputy for Development Planning

UNCLASSIFIED

SECURITY CLASSIFICATION OF THIS PAGE (When Data Entered)

REPORT DOCUMENTATION PAGE	READ INSTRUCTIONS BEFORE COMPLETING FORM
1. REPORT NUMBER: ASD/XR-TR-79-5029-Vol-I	2. GOVT ACCESSION NO.: AD-A084 225
3. RECIPIENT'S CATALOG NUMBER:	
4. TITLE (and Subtitle): TACTICAL TARGET ACQUISITION MODEL (TATAC) Analysts' Manual	5. TYPE OF REPORT & PERIOD COVERED: Volume I.
6. PERFORMING ORG. REPORT NUMBER:	
7. AUTHOR(s): Stewart Baily	8. CONTRACT OR GRANT NUMBER(s):
9. PERFORMING ORGANIZATION NAME AND ADDRESS: DIRECTORATE OF OPERATIONS RESEARCH, DEPUTY FOR DEVELOPMENT PLANNING, AERONAUTICAL SYSTEMS DIVISION (AFSC)	10. PROGRAM ELEMENT, PROJECT, TASK AREA & WORK UNIT NUMBERS: A2351/63101F
11. CONTROLLING OFFICE NAME AND ADDRESS: DIRECTORATE OF OPERATIONS RESEARCH (ASD/XROL), DEPUTY FOR DEVELOPMENT PLANNING, WRIGHT-PATTERSON AFB, OH 45433	12. REPORT DATE: Dec 77
	13. NUMBER OF PAGES: 70
14. MONITORING AGENCY NAME & ADDRESS (if different from Controlling Office): See Block 11.	15. SECURITY CLASS. (of this report): UNCLASSIFIED
	15a. DECLASSIFICATION/DOWNGRADING SCHEDULE: N/A

16. DISTRIBUTION STATEMENT (of this Report)

Approved for public release; distribution unlimited.

17. DISTRIBUTION STATEMENT (of the abstract entered in Block 20, if different from Report)

See Block 16.

18. SUPPLEMENTARY NOTES

19. KEY WORDS (Continue on reverse side if necessary and identify by block number)

Target Acquisition	Target Sensors
Tactical Air Power	Radar
Air-to-Ground Attack	Infrared
Atmospheric Effects	TV Systems
Tactical Scenarios	

20. ABSTRACT (Continue on reverse side if necessary and identify by block number)

A computer model for determining target acquisition capability of airborne sensors against ground targets is presented. The theory and general structure of the model plus details for the analyst are discussed. The model can be used to evaluate various types of electrooptical and radar sensors.

DD FORM 1 JAN 73 1473 EDITION OF 1 NOV 65 IS OBSOLETE

UNCLASSIFIED

SECURITY CLASSIFICATION OF THIS PAGE (When Data Entered)

403 975

PREFACE

This is one of two volumes of a report describing a target acquisition model developed under contract to Lulejian and Associates by the Deputy for Development Planning (XRO), of the Aeronautical Systems Division. The model was developed to support in-house studies of tactical air-to-ground attack.

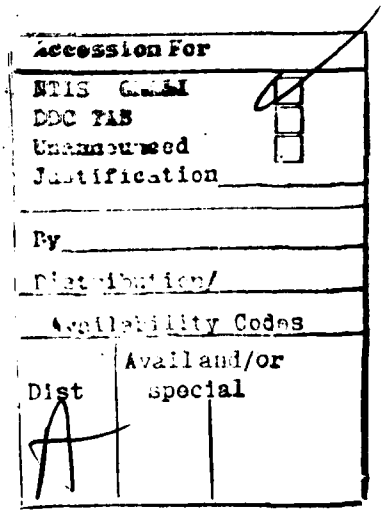

TABLE OF CONTENTS

TABLE OF CONTENTS (CONTINUED)

LIST OF TABLES

LIST OF ILLUSTRATIONS

TACTICAL TARGET ACQUISITION MODEL (TATAC)

I. GENERAL STRUCTURE OF THE MODEL

The general structure of the model is depicted in Figure 1. This is a minor modification to the form originally proposed by Bailey of The RAND Corporation (Ref 4), and used subsequently in the MARSAM II (Ref 13), and other models. It is attractive because it is easy to modify portions of the model to account for changes to sensor technology or to the dynamics of a specific search situation. Greening (Ref 3) embraces a sub-model segmentation of this sort.

A. DEFINITION OF TERMS

The approach considers the determination of separate conditional probabilities viz:

P_1 = The probability that an unobscured view of the target is presented to the observer.

P_2 = The probability that the observer will fixate on the area in which the target is located.

P_3 = The probability that the observer will have the threshold performance sufficient to discriminate the target at the required level of detail.

Formulations for these terms are drawn from those which have broad community acceptance. Where several equally acceptable formulations are available, those requiring the least amount of manipulation to produce the answer will be used. This is consistent with the implicit objective of the forthcoming mission analysis to understand the basic relationships driving the target acquisition/weapon delivery problem.

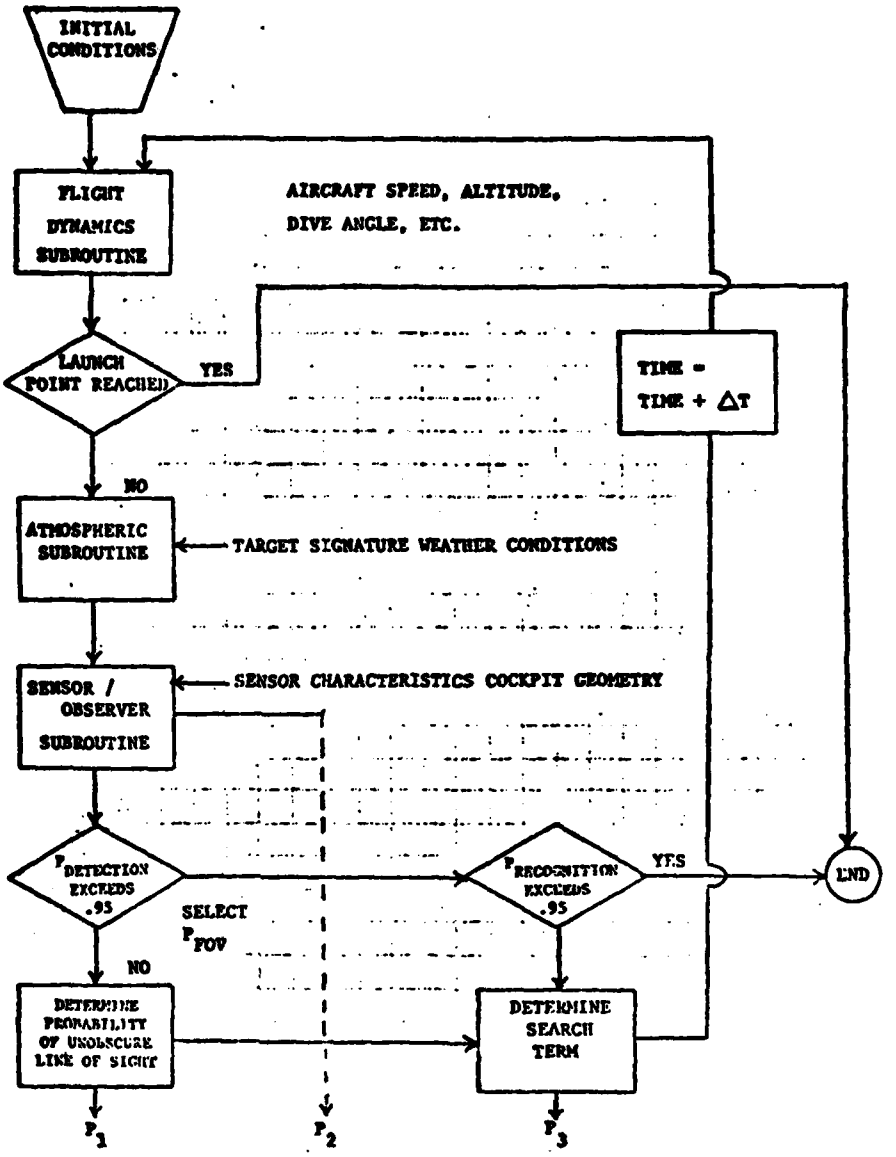

Figure 1. General Structure of the Model

The problem definition (i.e., guided weapon delivery on a pre-briefed target) permits some further simplification. Areas where the general applicability may be impacted because of the approximations/simplifications will be pointed out.

The problem entails the operational and technological alternatives to achieve a high probability of acquisition for a first pass weapon delivery; accordingly the model stops the problem when either the launch basket has been overflown or the cumulative probability of acquisition exceeds some specified value. The model can be used to evaluate seven forms of imaging sensors:

1. Unaided Visual (with or without cockpit masking constraints);
2. Forward-Looking Infrared (FLIR);
3. Active (illuminated) Television (ATV);
4. Passive (daylight) Television (PTV);
5. FLR - Moving Target Indicator Mode (FLR-MTI);
6. Forward-Looking Radar (FLR); and
7. Synthetic Aperture Radar (SAR), Squint or Side-Looking.

The radar subroutines (5), (6) and (7) may be exercised in sequence so as to simulate an advanced multi-mode radar such as the Advanced Tactical Radar (ATR). Thus, initial detection might be acquired using the real beam MTI mode and recognition achieved with the spotlight (synthetic aperture) mode.

B. LINE OF SIGHT CONSIDERATIONS (P_1)

There must exist an unobscured line of sight from the sensor to the target in order to image the target. The model considers three independent cases of physical opaqueness to target signature:

- Masking by terrain or cultural features (P_{unmask});
- Obscuration by cloud formations (except in the radar cases where the signal is attenuated but not obstructed (P_{CFLOS}); and

- Limits imposed by the sensor field of view or cockpit obstructions (P_{FOV}).

1. Masking by Terrain or Cultural Features

The model will consider this type of masking either probabilistically or deterministically. Cultural features can generally be rigidly defined for the scenario and, therefore, are more properly considered as deterministic inputs. Figure 2 depicts a typical form of cultural masking to be contended with in the tactical environment. The user defines the conditions which will satisfy the information requirements; i.e., in this case whether or not the revetment is occupied. The masking ratio is entered as an input to the program and a zero multiplier is applied to the P_1 term if these conditions are not satisfied. If no cultural masking value is input, the masking ratio defaults to a zero value.

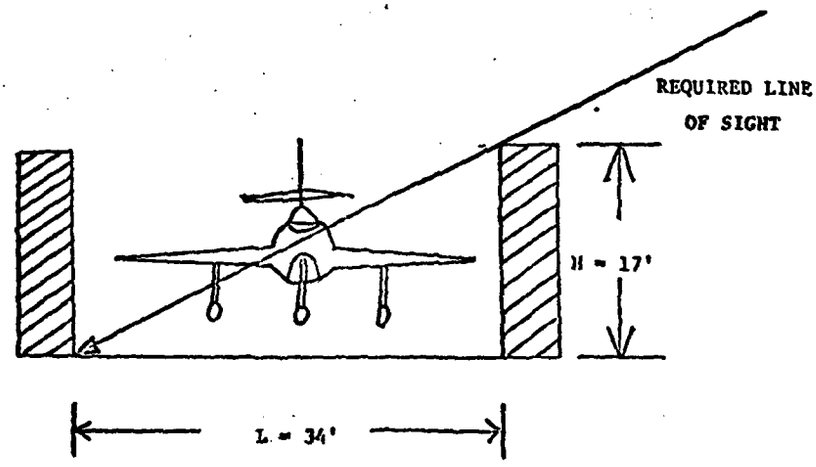

$$\text{MASKING RATIO} = \frac{H}{L} = .5$$

Figure 2. Masking Ratio - Cultural Masking (Aircraft in Revetment)

Terrain masking is entered in the form of an average masking angle value. The probability that the target will be unmasked to the sensor, P_{UNMASK}, is:

$$P_{UNMASK} = 1 - \exp(- \theta_D/\theta_{AV}) \quad (1)$$

where:

θ_D = Angle between LOS and ground plane

θ_{AV} = Average masking angle

The above formulation is taken from a recent reconnaissance study (Ref 16), and is based on typical tactical situations. The results for an 8° masking angle compare very closely with the precise measurements made by US Army engineers for the JTF-2 Low Altitude Acquisition Tests. Other values used widely are presented in Table 1.

TABLE 1. REPRESENTATIVE VALUES FOR AVERAGE TERRAIN MASKING ANGLE (CENTRAL EUROPE)

AVERAGE ANGLE θ_{AV}	SCENARIO
.5°	Airfields or Port Areas.
1.5°	Suburban Areas in which Manufacturing or Transportation Center would be Located.
8°	Forested Rural Areas.
45°	Highways Connecting Urban Areas.

2. Obscuration by Cloud Formations

Table values are employed in the model to determine the instantaneous probability that the sensor to target path is cloud free.

The values vary with the location, time of day, and season. Figure 3 presents the high and low altitude cases provided as options in the model. These data were reported for altitudes of 5000 and 30,000 feet in the referenced ETAC report. The user may respecify either one of these curves by entering a data point for each 30° of zenith angle. The program performs a linear interpolation between points.

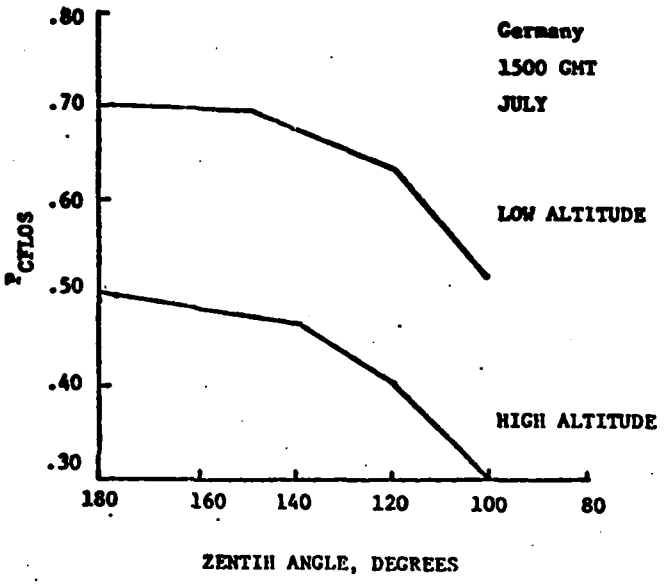

Source: ETAC # 6467

Figure 3. Impact of Clouds on Target Acquisition

3. Limits Imposed by a Sensor Field of View or Cockpit Obstructions

Information on the target location given to the pilot is inaccurate. Errors are introduced in the prior reconnaissance and targeting process on the order of 50-500 feet (CEP) depending on the system employed. This area of uncertainty may grow with time if the target is mobile. There are additional errors introduced in pointing the reacquisition sensor because of the uncertainty in the location of strike aircraft relative to the original targeting grid.

The model addresses two operational modes of sensor search: (a) a variable depression angle search in which the sensor is continuously pointed toward the center of the pilot's best estimate of the target location, and (b) a fixed depression angle search in which the pilot preselects a depression angle and scans the displayed area for the appearance of the target.

a. Variable Depression Angle Search

When the location of the target is known with reasonable accuracy, the pilot may direct the sensor at the suspected area at all times during the approach to the target. If the field of view is constant, this has the effect of presenting a smaller and smaller sensor "footprint" as the target is approached. In other words, likelihood that the target will not be within the field of view will increase montonically with time.

Assuming that the cross-track and along-track errors are independent, normally distributed, and that their standard deviations are specified separately, the probability that the target will be in the field of view of the sensor at range r is given by:

$$P_{FOV}(r) = \frac{1}{2\pi} \int_{-X(r)/2\,\sigma_x}^{X(r)/2\,\sigma_x} \exp(-u^2/2)\,du \int_{-Y(r)/2\,\sigma_y}^{Y(r)/2\,\sigma_y} \exp(-v^2/2)\,dv \qquad (2)$$

where:

X(r) = The width (cross-track) of the area covered by the field of view of the sensor at range r, measured at the center on the ground.

$Y(r)$ = The length (along-track) of the area covered by the field of view of the sensor at range r, measured at the center on the ground.

σ_x = Standard deviation of the cross-track error.

σ_y = Standard deviation of the along-track error.

b. Fixed Depression Angle Search

This case is typical of a search and destroy mission in which little information is available on the target location. The display search area is a constant value. This is also typical of the visual search case in which the pilot's view of the ground is fixed by the limits of the horizon and cockpit masking. The P_{FOV} term is deterministic (0/1) in nature. The model evaluates the amount of time in which the target is not opaque to the sensor.

C. THE SEARCH TERM

Fairly good agreement exists in the community with regard to the nature of all but the P_2 (search) term. This is because the search process is highly scenario dependent. One extreme is bounded by the random search case in which the observer searches uniformly over a wide area. Such search might properly characterize aerial surveillance of an ocean area. The opposite extreme is one in which a priori information exists on the target as to the probable nature of the location (e.g., along a road). In these cases, which are more characteristic of the Air Force strike problem, the observer will allocate a higher proportion of time to high-payoff search areas.

Bailey (Ref 4) has developed a formulation for P_2 which can be applied to either the visual or aided search situation. The terms presume a random search situation; however, with minor manipulation a scenario entailing different degrees of a priori targeting information can be created. The equation proposed by Bailey:

$$P_2 = 1 - \exp\left[(-700/G)(a_t/a_s)\Delta t\right] \quad (3)$$

where:

P_2 = The probability that the observer will look in the direction of the target with his foveal vision during the time increment.

a_t = The area of the target projected in a plane normal to the observer.

a_s = The area to be searched, projected likewise.*

G = A measure of scene complexity.

Δt = Time spent searching the target area.

It is apparent that a_s could be defined simply by the constraints of cockpit masking. It is equally apparent that a_s can be reduced through the use of cueing information. With perfect targeting and navigation by the search aircraft, P_2, approaches unity. Cases for specific scenarios can be formulated by geometric evaluation. For example, if the target were known to be along a certain road, a_s, could be defined to be the

* In the case of EO-aided acquisition, the areas are normally those resulting from the ground footprint of the field of view selected by the operator. Options are provided in the model to use any portion of the surrounding area of the target in the definition of a_s, however.

viewable area along the road as bounded by cockpit masking and other LOS constraints. Figure 4 depicts the geometry.

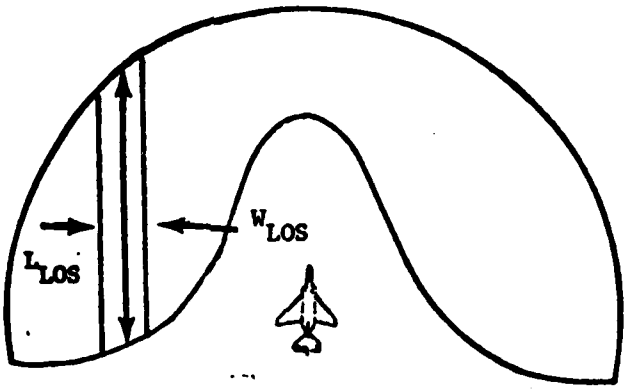

COCKPIT MASKING

DETERMINATION OF a_s FOR VISUAL LOS SEARCH SITUATION

Figure 4. LOS (Masking, Horizon or Other Criteria).

The model considers the impact of multiple targets in the P_2 term for the linear search case. The effective target area for search is increased such that:

$$a_t = a_t \left[(N_t + (N_t-1)S_t)/L_t \right] \quad (4)$$

where:

N_t = Number of targets.

S_t = Spacing between targets.

L_t = Target length.

The detectability (P_3) Term) of the target array is based on the individual element dimensions. A check is made to assure that the ground

resolution in the along-track dimension, Dgx, is sufficient to discriminate separate targets, i.e.: $Dgx \leq S_t$.

The value of G, which is a measure of the increase in the number of fixation centers as the scene becomes more complex, typically varies between one and ten. Bailey had hoped that controlled field tests would be performed which would determine its value for different search situations. Since such tests did not materialize, the limited laboratory data of Rosell (Ref 7) will be used. Although the latter tests were performed primarily to quantify the effects of clutter, there is a casual relationship between complex scene situations and clutter. Thus, G will enter the EO system's performance determination as well. The proposed values for G and a discussion of their derivation is provided in Section 3.A.

D. DISCRIMINABILITY (P_3)

Two levels of discrimination are considered pertinent for tactical usage:

1. Detection - Determination of the location of non-natural objects of potential military interest; and
2. Recognition - Categorization of objects by classes such as tanks, aircraft, etc.

It is obvious that the lower level of discrimination must occur before the cognitive process of classification can commence. It is equally apparent that in some cases there may exist sufficient contextual detail such that detection level resolving performance is equivalent to recognition in terms of information content.[1] The user must consider carefully

[1] The distinctive geometric arrangements of surface-to-air missile launchers and the fire control van is an often-cited example of tactical contextual detail.

the nature of the target area scene to decide on the level of discrimination required for a given tactical task.

The level of disciminability in this model is determined by the target spatial and spectral signature. The spectral signal-to-noise ratio must, of course, exceed the threshold required for sensor performance. The reaction of the human observer to the displayed signal is determined on the basis of psychophysical data relating performance to the size and contrast of the target.

There is a dearth of useful experimental data on the image enhancement achieved with certain targets having unique spectral signatures. For example, combat tanks have engines in the rear and, while moving, can be distinguished from similarly sized trucks when viewed in IR spectrum before the distinguishing features of the turret are resolved. These important but unquantifiable advantages of the sensing spectrum are ignored in the model. Similarly, discriminability based on color in the visible light portion of the spectrum is not treated. All but the blue-green wavelengths are attenuated at the slant ranges required for guided weapon delivery, hence color as a discriminate is of questionable value. The impact of color filters has been ignored because recent experimental evidence (Ref 5) suggests that there is little, if any, overall improvement in observer response with their use.

The basis for relating human performance to spatial resolution is traced back to the work of John Johnson of the US Army Night Vision Laboratories (Ref 6). Johnson determined that, given "sufficient" signal-to-noise, observers could detect or recognize an object at the 50 percent performance level when either approximately two or eight TV lines were

available, respectively, across the minimum target dimensions. This is equivalent to a photographic resolution of one or four pairs of black and white bars. The concept of an equivalent bar pattern, as depicted in Figure 5 for a target with minimum linear dimension Y, was established by Rosell of the Westinghouse Corporation (Ref 7). Signal-to-noise and spatial frequency requirements are considered simultaneously in Rosell's work, which will be covered in more detail in the section on raster scanning sensors. In the radar case and in the case of unaided visual performance, a threshold signal-to-noise value will be established for detection.

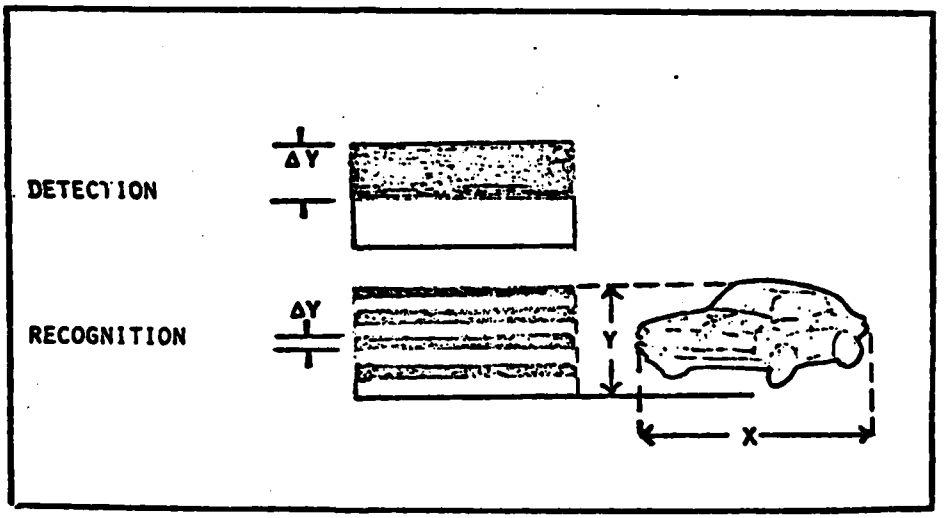

Resolution Required per Minimum Object Dimension to Achieve a Given Level of Object Discrimination Expressed in Terms of an Equivalent Bar Pattern

Figure 5. Equivalent Bar Pattern Concept

Recognition performance will be based purely on spatial frequency content as stipulated by Johnson's criteria.

E. DYNAMICS OF ACQUISITION

Before the terms for combining the separately determined probabilities are presented, it is worthwhile to consider the nature of the problem and the origin of the psychophysical data on which separate terms are based. Tactical target acquisition is a process which occurs over a very small period of time relative to usual periods in which human performance are measured. While in the long run it may be allowed that the individual variability in response to stimuli within the population is small, it is generally agreed that an individual's performance varies significantly from hour to hour. The amount of rest and emotional state among other things determine the threshold level at which the individual will react.

Thus, when psychophysical data are summarized in the form of a continuous distribution, it is apparent that each point represents a proportion of subjects which will react to the level of stimulus. If, for example, it is determined that 30 percent of the population will detect a high contrast object at a certain distance, then the maximum probability of detection, given that an observer is selected at random, is 0.30. In the case of tactical target acquisition the pilot is chosen before the flight and cannot be changed enroute. Thus, the only time-accumulative term to be considered is the probability that the observer's vision is directed at the area in which the object is located.

With this concept in mind, consider a case in which observers selected at random approach a target at a constant speed. If there are no anomalous conditions regarding the atmosphere or the acquisition geometry, both target size and contrast will increase during the approach. Thus, the proportion of observers that are capable of seeing target, P(r), will increase montonically with diminishing range as depicted in Figure 6.

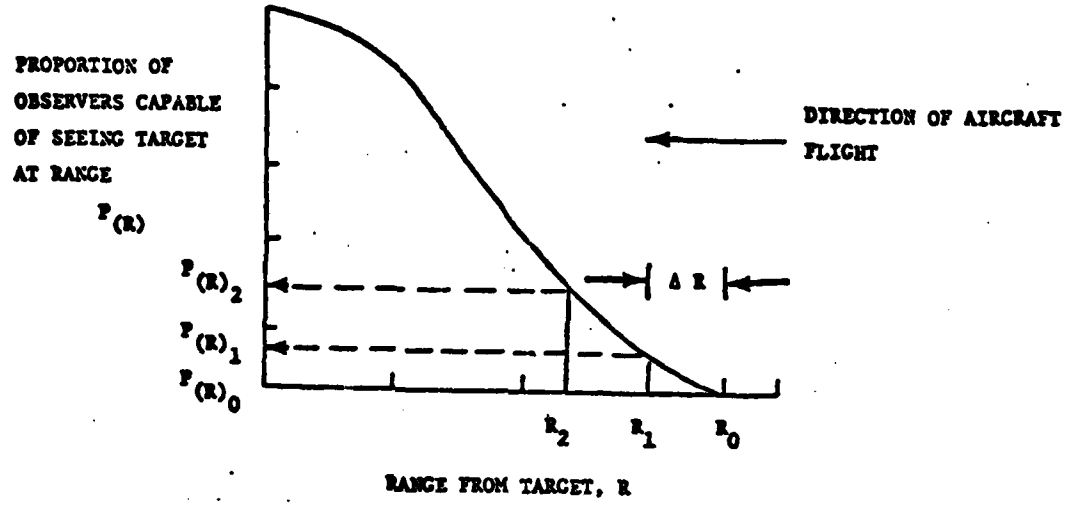

Figure 6. Evaluation of Acquisition Dynamics

For illustrative purposes, the abscissa can be divided into range increments Δr so that:

$$\Delta r = V G_t \tag{5}$$

where:

V = Velocity of aircraft (Ft/Sec).

G_t = Glimpse time (Sec).

A proportion of the population $P_{(r1)}-P_{(r0)}$ have threshold performances which, if their glimpse is directed at the target, will result in a detection. The probability that a mission flown by a pilot selected at random from the population will achieve acquisition at range r_1 is then:

$$Pa_{(r1)} = [P_{(r1)} - P_{(r0)}] P_g \tag{6}$$

where:

P_g = The conditional probability that at least one glimpse falls on the target.

In the next Δr increment a larger proportion of the population can discriminate the target. Of this proportion, the capable group $[P_{(r1)} - P_{(r0)}]$ will have had two glimpse opportunities while the capable group $[P_{(r2)} - P_{(r1)}]$ will have their first. The probability that the mission will have achieved acquisition by range r_2 is:

$$Pa_{(r2)} = [P_{(r1)} - P_{(r0)}] [1-(1-P_g)^2] + [P_{(r2)} - P_{(r1)}] [1-(1-P_g)^1] \quad (7)$$

Equation (7) is a geometric progression which is appropriate for search situations in which the P_g is a constant and the glimpse opportunities are independent. Real-life search situations are complicated by a number of interdependent considerations, viz:

1. P_g is found to be dynamically changing with range r, since the target size relative to the search area size is increasing with diminishing range. This impact is readily apparent from examining the parameters in the search term P_2 (see Section 1-C);

2. Masking by cultural/terrain features and obscuration by cloud formations becomes less severe as the look angle improves. On the other hand, the size of the sensor ground footprint grows smaller with decreasing range, thus, reducing the probability that the target will be contained within the field of view. These effects (P_{UNMASK}, P_{CFLOS}, P_{FOV}), collectively, make up the P_1 term defined in the previous section; and

3. Finally, the $P_{(r)}$ term may change because of the level of information required may be different at different portions of the flight profile. The notations for the two levels stipulated in the previous section, detection and recognition, are P_{3D} and P_{3R}, respectively.

Generalizing the dynamic acquisition formulation and rewriting in the notations of the terms defined previously, the cumulative probability of acquisition after M glimpse opportunities is*:

$$Pa_{(r)} = \sum_{i=1}^{M} (P_{3_i} - P_{3_{i-1}})(P_{1_i} P_{2_i} + \sum_{j=i+1}^{M} P_{1_j} P_{2_j} \prod_{k=i}^{j-1} (1-P_{2_k})) \qquad (8)$$

* Several steps in the development of this equation have been omitted because of space limitations. The full expansion is given in Ref 7.

II. UNAIDED VISUAL PERFORMANCE

A. THRESHOLD PERFORMANCE

Koopman [1946] developed the formulation for contrast threshold performance of the observer in terms of target size in the form:

$$C_t = K_1 \theta^{K_2} + K_3 \theta^{K_4/\alpha^2} \quad , \theta > .8° \tag{9}$$

where:

θ = Angle subtended by the eye in degrees between the point of fixation and the target.

α = Average angular diameter of the target at the eye in minutes of arc.

C_t = Threshold contrast for a given performance level (e.g., 50 percent, 90 percent, etc.).

K_1, K_2, K_3, K_4 = Empirical constants determined for the observer group.

A number of experimenters have determined the constants for Equation (9). In all cases the visual detection lobe so defined is a cone shaped volume with proportions similar to Figure 7. It is apparent that in the

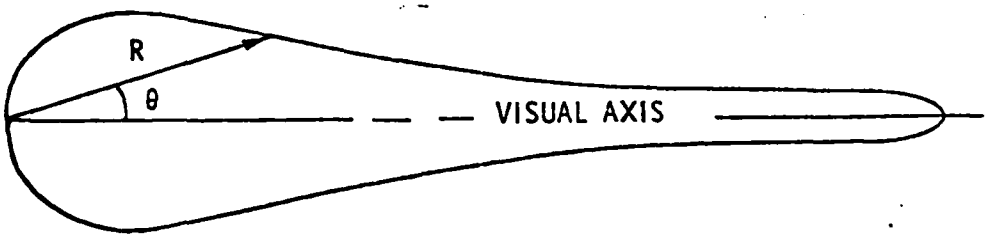

R Defines Target Angular Diameter and Apparent Contrast
The Threshold Contrast, C_t, used in the Model:

$$C_t = .0265\,\theta^{.24} + \frac{.440^{1.6}}{\alpha^2} \quad , \theta \geq .8°$$

Figure 7. Visual Detection Lobe

case of vigilant search, detection will most likely occur when the narrow axis of the lobe sweeps the target. The threshold contrast of the target when viewed foveally ($\theta \leq .8°$) is therefore of interest. The 57 percent performance level as determined by Koopman for the foveal case is:

$$C_t = 0.157 + .152/\alpha^2 \tag{10}$$

Equation (10) establishes the expected performance of a group of observers to discriminate the target from its background under ideal conditions. The use of Koopman's data tends to predict detection ranges significantly greater than those obtained in controlled field tests. Researchers at CALSPAN (Ref 9) have fitted Equation (9) with a new set of constants based on the experiments conducted by Sloan [1961], and obtained results which more closely conformed to a limited set of flight profiles examined. The resulting set of constants which are employed for this model are:

$$K_1 = 0.0265$$

$$K_2 = 0.24$$

$$K_3 = 0.44$$

$$K_4 = 1.6$$

The equation to obtain the probability distribution with apparent contrast is*:

$$P_{3_D} = 0.57 + K\{1 - \exp[-4.2(C_a/C_t - 1)^2]\}^{1/2} \tag{11}$$

where:

P_{3_D} = The proportion of observers which can discriminate a target at the specified angular subtense and size.

* This is the algebraic approximation to Blackwell's data used by Bailey in The RAND model.

C_a = Apparent contract.

$$K = \begin{cases} -.57, & C_a/C_t \leq 1 \\ +.43, & C_a/C_t \geq 1 \end{cases}$$

B. HIGHER LEVELS OF DISCRIMINATION

As mentioned in Section D, the experimental basis for determining the number of resolution elements required to obtain a given level of information is drawn from the work of Johnson at the Night Vision Laboratories. The model employs the analytic approximation of Johnson's criteria in the MARSAM model fitted to some data by Brainard [1965]. This presumes that the target shape is the principal identifying feature. The equations are:

$$P_{3R} = 1 - \exp\left[-(NR - 3{\cdot}2)^2/11\right], \quad NR \geq 3{\cdot}2 \qquad (12)$$

$$P_{3R} = 0, \quad NR < 3{\cdot}2$$

where:

NR = The number of lines of resolution across the minimum target dimension.

The effective resolving performance of the eye has been determined to be about three minutes of arc in static situations, increasing with the cube of the angular velocity of the target with respect to the observer.

Very high angular rates blur the image, affecting the effective resolution of the eye. Simulator studies at North

American (now Rockwell International) have established the following relationship:

$$NR = 2 \{\alpha / [3 + (2{\cdot}9 \times 10^{-6}) V_a^3]\} \quad (13)$$

where:

α = Angular subtense of the target in minutes of arc.

V_a = Angular velocity in degrees/sec.

III. PERFORMANCE OF RASTER SCANNING SENSORS

A. GENERAL

Rosell, under the sponsorship of the Air Force Avionics Laboratory (AFAL), has developed models which provide considerably deeper insight into the relative impact of system components on the overall performance of a sensor to provide the required level of imagery detail. The theory is documented in detail in reference 6. This section summarizes the key relationships presented in those documents. Approximations to some relationships were made for ease of machine computation where prudent. The author benefitted from the prior work of Tom Lippiatt of The RAND Corporation, Bud Minelli of ASD/ENA, and Dave Shumaker of Systems Consultants, Inc., who had previously implemented models using the basic theory for passive TV, active TV, and FLIR systems, respectively. Portions of a static FLIR model developed by Phil Miller, ASD/ENA were also adapted.

The central formulation in the Rosell model is based on his conclusion that an observer viewing a display is signal-to-noise limited. The proportion P(r) of observers who can see the target at range (r) is therefore:

$$P_{(r)} = \frac{1}{\sqrt{2\pi}} \int_{-\infty}^{[SNR_D(r) - SNR_{DT}(r)]} \exp(-u^2/2)du \qquad (14)$$

where $SNR_D(r)$ is the signal-to-noise at the display and $SNR_{DT}(r)$ is the threshold signal-to-noise ratio at the display, defined as that signal-to-noise ratio SNR_{DT} for objects on various backgrounds as a

function of spatial frequency obtained from a set of psychophysical experiments performed in the laboratory.

The required spatial frequency can be related to the viewing geometry and the level of discrimination (i.e., detection or recognition). Thus, Figure 8, combined with a measure of system signal-to-noise, SNR_D, under a given set of environmental conditions, may be used to predict the proportion of observers capable of acquiring the target. SNR_{DT} is a summary measure of image quality.

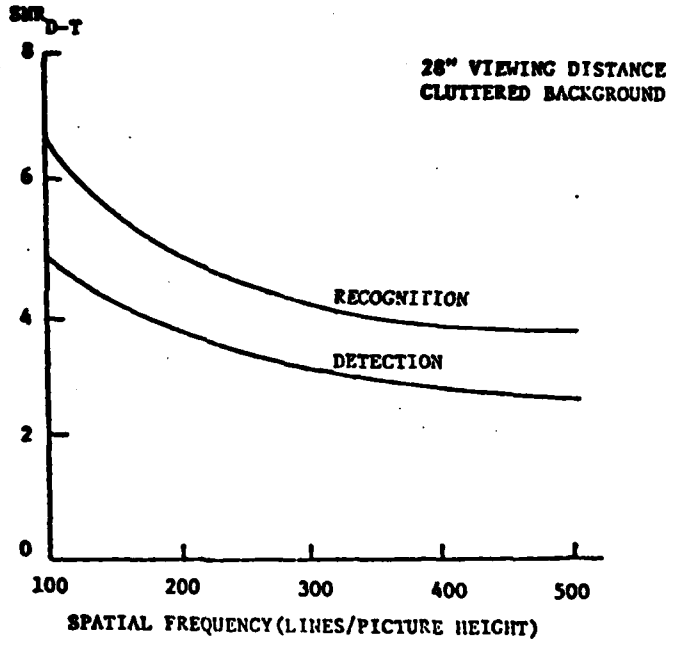

Figure 8. Threshold SNR_D as a Function of Spatial Frequency

Rosell conducted further experiments to determine the increase in SNR_{DT} required as the scene complexity increased. He found a 15 percent increase for vehicles on a road, a 25 percent increase for vehicles in the grass and bushes, and a 50 percent increase for

vehicles in the trees. Lippiatt has suggested the use of Bailey's "G" factor as a surrogate quantitative measure of the increase in SNR_{DT} demanded in different tactical situations. Using this concept, we may approximate:

$$SNR_{DT}(r) = [6.18 \exp(-.00252\ N(r))]\ [1 + .008\ G^2] \quad (15)$$

for detection, and

$$SNR_{DT}(r) = [8.20 \exp(-.00248\ N(r))]\ [1 + .008\ G^2] \quad (16)$$

for recognition.

Equations 15 and 16 hold reasonably well for $N(r) \leq 300$. A straight line approximation to the respective curves in Figure 8 is used otherwise.

Considering the limited sample set of observations in the psychophysical experiments, a more precise fit to the data is not justified. This portion of the model could and should be revised as more laboratory data becomes available. Table 2 is proposed for the selection of "G" values. These values were derived by the author by substitution in Equations (15) and (16) to reproduce the experimental data obtained thus far.

TABLE 2. "G" VALUES

G	DEGREE OF SCENE COMPLEXITY
2	Search in Essentially Featureless Areas such as a Desert or Open Ocean Area.
4	Search Along a Line of Communication.
6	Search in Open Meadow Areas.
8	Search in Forested Areas.
10	Search in Complex Mixtures of Cultural and Terrain Features.

Both image and noise may be described by a photon density on the display surface. Since the observer can spatially integrate the image, the signal is proportional to the area of the image. The mean square noise is also proportional to the image area.

The signal-to-noise ratio of the target at the display, $SNR_C(r)$, as developed by Rosell for TV systems, expressed in terms of a mean signal to root mean square noise, becomes then:

$$SNR_{DT}(r) = \left[\frac{\eta_v t}{\alpha \xi_y(r)}\right]^{1/2} \frac{2R_{SF}[N(r)]C_m}{N(r)} \qquad (17)$$

$$\frac{G_T i_{ave}}{[G_T^2\, \beta_T(r)\, \Gamma_y(r)\, i_{ave} e + I_p^2/2\Delta f_v]^{1/2}}$$

where:

η_v = Projected width to length ratio of the target $\frac{W_T}{l_T}$

t = Integration time of the eye

α = Picture tube horizontal to vertical aspect ratio

e = 1.6×10^{-19} coulomb the charge of an electron

I_p = Pre-amp noise in amps

Δf_v = Bandwidth (Hz)

G_T = Gain of sensor tube

C_m = The modulation contrast at the sensor

i_{ave} = Average photo surface current (ampere)

R_{SF} = Square wave flux response at spatial frequency $N_{(r)}$

N(r), the required television lines per picture height for a given level of discrimination is:

$$N(r) = \theta_v K/\alpha_T(r) \tag{18}$$

where: θ_v is the verticle field of view of the sensor, $\alpha_T(r)$ is the angle subtended by the minimum dimension of the target at the sensor, and K is a constant equal to two for detection or equal to eight for recognition (based on Johnson's criteria).

The signal-to-noise ratio of the target at the display for FLIR systems is based on the work by Sendall (Ref 9). Further development by Biberman (Ref 10), and Shumaker (Ref 11) suggest that the equivalent term for Equation 17 is:

$$SNR_D(r) = \left[\frac{\eta_v}{7N^2(r)A\alpha}\right]^{1/2} \frac{R_{SF}[N(r)]\Delta T\ T_a}{NET} \frac{(\dot{F}\ R_{os}t)^{1/2}}{\sqrt{\rho}} \tag{19}$$

where the additional terms are:

ΔT = Absolute temperature difference between the target and its background.

T_a = Atmospheric transmissivity.

NET = Noise equivalent temperature difference.

$\dot{F}$ = System frame rate.

R_{os} = Overscan ratio.

ρ = Bandwidth ratio.

A = Area of detector.

The following sections will develop the terms for the TV (passive and active), and FLIR systems. Since much of the technology of FLIR systems is based upon TV, the latter terms will be developed first, followed by those modifications and additions required for FLIRs.

B. TV SYSTEMS

If the overall MTF (sine wave response) of a sensor is $R_o[N_{(r)}]$,

the overall response of the sensor to a unit amplitude square wave in the x direction may be written in terms of a Fourier transform:

$$g(x) = 1/2 + 2/\pi \sum \frac{R_o(N(r)K]}{K} \cos [\pi N(r) K x] \qquad (20)$$

where: g(x) is normalized to unit amplitude at N = 0. Rosell postulates that the observer, in detecting the presence of a bar pattern must make his decision on the basis of detecting a single bar, and that the signal associated with the bars in the x direction is proportional to the mean signal amplitude which will be designated the square wave flux response $R_{SF}(N_{(r)}]$.* The mean value of g(x) is:

$$R_{SF}[N(r)] = 4/\pi\ N(r) \sum \frac{R_o[N(r)K]}{K} \int_{-1/2\ N(r)}^{1/2\ N(r)} \cos[\pi N(r)\ K\ x]\ dx \qquad (21)$$

Equation 20 implies that the number of bars in the bar patterns are sufficient so that the pattern's Fourier spectrum approaches a line and that any end effect transients are damped out.

The sine wave modulation transfer function $(R_o(N)]$ is approximated, based on the work of Hall (Ref 7 by:

$$\begin{aligned} R_o N(r) &= \exp(-4.4N^2/N_E^2) \quad , N \leq N_o/3 \\ &= (\pi/4) \exp(-3N^2/N_E^2) \quad , N > N_o/3 \end{aligned} \qquad (22)$$

where:

N_o = the one percent effective frequency response (approximately 1.24 times N_E, the 5 percent limiting response).

* A vertically oriented bar pattern is aperiodic in the y direction along the length of the bars and periodic in the x direction across the width of the bars. The lens and photo surface apertures distort the input pattern with the major effects in the periodic direction.

The modulation transfer function of the lens system $R_L(N)$ is given as:

$$R_L(N) = 1/\pi\ (2\beta - \sin 2\beta) \tag{23}$$

where:

$$\cos \beta = [N\lambda f(1+\alpha)^{1/2}] \ / \ [2000d]$$

and:

λ = Wavelength of interest

d = Diameter of lens

f = Optical f/number

If an imaging system is linear, the response (displayed image) to a periodic test pattern will also be periodic with the spatial frequency as the test pattern. The primary effect of an aperture on a periodic pattern in the direction across the bars is to reduce signal, leaving noise unchanged. However, the noise will be filtered by the aperture if it follows the point of noise insertion. The noise filtering factor β_T for filtering photoelectron noise in the periodic direction is given by:

$$\beta_T = 1/N(r) \int_0^{N(r)} [R_o(N)]^2 \ dN \tag{24}$$

where $R_o(N)$ represents the product of all of the MTFs which follow the point of noise insertion.

For ease of computation β_T is approximated in the program for $N(r) \leq N_o/3$ by :

$$\beta_T(r) = (3\ N_E/N(r)\ )\ \mathrm{erf}[3\ N(r)/N_E] \tag{25}$$

and for $N(r) > N_o/3$ by :

$$\beta_T(r) = (N_E/N(r)\ )\ [.086 + .223\ \mathrm{erf}[2.45\ N(r)/N_E] \tag{26}$$

The correction factor, $\xi_y(r)$ for increased noise in the aperiodic direction due to enlargement of the image by the lens and the tubes target is given by:

$$\xi_{(r)} = [1 + (N(r)/\eta_v N_{eL})^2 + 2\ (N(r)/\eta_v N_{eT})^2]^{1/2} \tag{27}$$

The correction factor, $\Gamma_y(r)$ for filtering photo-electron noise in the aperiodic direction by the target is given by:

$$F_y(r) = \xi_y(r)\ /\ [1 + (\ N(r)\ /\eta_v\ N_{eL}\ )^2 + 2\ (\ N(r)\ /\ \eta_v\ N_{eT})^2\ ]^{1/2} \tag{28}$$

The noise equivalent passband for the tube (N_{eT}) and for the lens system (N_{eL}) are given by:

$$N_{eT} = .31\ N_E$$

$$N_{eL} = (\ 545\ d\ )\ [\ \pi^2 f(1+\alpha^2)^{1/2}\ ] \tag{29}$$

The square wave flux response, $R_{SF}[N(r)]$ for the system thus becomes

$$R_{SF}[N(r)] = 16/\pi^3 \sum_{K=1}^{K\ N(r)\leq N_o/3} \frac{\cos^{-1}\phi - \phi(1-\phi^2)^{1/2}]\exp[-4.4\ N(r)^2/N_E{}^2]}{K^2} + 4/\pi^2 \sum_{K\ N(r)>N_o/3}^{K\ N(r)>N_0} \frac{\cos^{-1}\phi - \phi(1+\phi^2)^{1/2}]\exp[-3\ N(r)^2\ /\ N_E{}^2]}{K^2} \quad (30)$$

where $\phi = N(r)\ \lambda\ f\ (1+\alpha^2)^{1/2}\ /2000d$

For passive TV systems, i_{ave}, the average photo-surface current is given by:

$$i_{ave} = A\ [\sigma\rho_{ave}\ H_s\ /\ 4(f/T_o)^2\ ]^{\gamma} \quad (31)$$

where:

ρ_{ave}	=	The average background reflectance
γ	=	The slope of the signal current vs/irradiance characteristic
A	=	Effective photo surface area (m^2)
H_s	=	Solar irradiance (watts/m^2)
σ	=	The average radiometric responsibility of the tube
T_o	=	Transmittance of the lens system

A is given by:

$$A = \alpha d^2 / (1+\alpha)^2 \qquad (32)$$

For illuminated systems, equation (31) is modified to:

$$i_{ave} = A \left[\sigma \rho_{ave} P_i T_{at} / 4 A_s f^2 T_o R^2 \right]^{\gamma} \qquad (33)$$

where:

P_i	=	Effective power out of the illuminator (watts)
A_s	=	Illuminator beam solid angle in steradians
R	=	Slant range to the target
T_{at}	=	Atmospheric transmissivity at range R in the appropriate region of the electromagnetic spectrum

C. FLIR SYSTEMS

Current FLIR systems are typically specified in terms of a Mean Resolvable Temperature (MRT). The MRT is measured at the display and is for a target of known spatial frequency, that temperature difference which is resolvable at the observer 50 percent performance level.

It is apparent from the definition of MRT that the SNR_{DT} should equal the values determined by Rosell for a given spatial frequency N(r) when the apparent target temperature difference is equal to the MRT. Proceeding from the basic formulation for radiant emittance, W, $W = \sigma_B T^4$ where

T = Equivalent blackbody temperature.

σ_B = The Stefan Boltzman Constant

Miller (Ref 11) provides an equivalent expression for Equation (17):

$$SNR_D(r) = [SNR_{DT}(r) \left| T_t^4 - T_b^4 \right| T_a] / [T_m^4 - T_1^4] \quad (34)$$

where:

T_a	=	Atmospheric transmittance
T_t	=	Equivalent temperature of the tactical target (°Kelvin)
T_b	=	Equivalent temperature of the background
T_m	=	Equivalent temperature of the MRT target
T	=	Equivalent temperature of the MRT target background (normally 300°K)

By definition

$$T_t - T_b = \epsilon_t t_t - \epsilon_b t_b \quad (35)$$

ϵ_t	=	Emissivity of the target
ϵ_b	=	Emissivity of the background
t_t	=	Absolute temperature of the target
t_b	=	Absolute temperature of the background

and:

$$MRT = \left| T_m - T_1 \right| \quad (36)$$

for the spatial frequency of interest. Therefore the equation (34) is approximately equal to:

$$SNR_D(r) = \frac{SNR_{DT}(r)\ \varepsilon_t t_t - \varepsilon_b t_b}{MRT(r)} \left(\frac{\varepsilon_b t_b}{300}\right)^3 T_a \qquad (37)$$

The MRT target has typically a 7/1 bar length to width ratio. The $SNR_{DT}(r)$ corrected for aspect and viewing distance corresponding to laboratory conditions for a vertically oriented bar pattern may be approximated by:

$$SNR_{DT}(r) = [5 \exp(-.00183\ N(r))]\ [7\ \eta_v]^{-1/2} \qquad (38)$$

If the determination of MRT is conducted with no constraints on the positioning of the head with respect to the display, the $SNR_{DT}(r)$ corresponding to an optimum observer to display distance should be used. Equation (38) would then be replaced by:

$$SNR_{DT}(r) = [3 - .002\ N(r)]\ [7\ \eta_v]^{-1/2}$$

where:

η_v = The Tactical Target Apparent width to length ratio.

Equations (34) and (37) represent the obtainable and demand signal-to-noise at the display, respectively, which may be substituted in equation (14) to obtain P(r), the proportion of observers who can discriminate the target at range (r).

IV. RADAR SYSTEMS

The mathematical representation of the radar systems employed in this model has been drawn almost in its entirety from the MARSAM model (Ref 12). Since the system documentation covers in detail the theoretical basis for the terms and algorithms in that model, only the fundamental relationships and the changes made to account for new technology since the implementation of MARSAM II [1968] will be covered here.

A. REAL BEAM RADARS

The basic equation for range performance fundamental to all radar systems in terms of power density returned to the platform, I(r) is:

$$I(r) = P_t G_o \sigma_\lambda / (4\pi)^2 R^4 \quad (39)$$

where:

R	=	The Target to Radar Distance
P_t	=	Effective Transmitter Power
G_o	=	Gain of the Radar Antenna
σ_λ	=	Radar Cross Section of Target

Since the pulses can be emitted no more frequently than the time required for the radiation to travel to the target and return, the theoretical maximum range of the radar, R_m, is:

Since the pulses can be emitted no more frequently than the time required for the radiation to travel to the target and return, the theoretical maximum range of the radar, R_m, is:

$$R_m = C / 2 f_p \quad (40)$$

where:

C	=	The speed of light
f_p	=	Pulse repetition frequency

Azimuth resolution may be determined analytically by the relationship:

$$\theta_h = \lambda / a \quad (41)$$

where:

λ	=	Transmitted wavelength
a	=	Antenna aperture

The antenna apertures for tactical aircraft are limited to about 3 feet in diameter. Radar frequencies suitable for operational usage vary between 10-20 Ghz. Typical air-to-ground radars provide angular resolutions on the order of 1.5°-3°. The ground resolved azimuth dimension for a FLR, Dgx, is:

$$D_{gx} = R \theta_h \quad (42)$$

where:

R	=	Slant Range (feet)
θ_h	=	Horizontal antenna beamwidth (radians)

Thus the typical resolution mentioned above would provide about 400-800 feet ground resolution at a 5 nm slant range.

Range resolution is a function of the pulse width and the depression angle. Specifically:

$$D_{gx} = C\, T_{pw} / 2 \cos \theta_d \qquad (43)$$

where:

C	=	The speed of light (feet/sec)
T_{pw}	=	Pulse width (seconds)
θ_d	=	Depression angle (degrees)

These familiar equations govern the signal return of both the target and the target surroundings (clutter). They are presented exclusive of the numerous receiver plumbing losses and atmospheric attenuation effects.

The MARSAM FLR model determines target detectability on the basis of a threshold signal-to-clutter ratio (nominally 15 db). This value is based on the sensitivity in the receiver electronics and is normally set so that the probability of a false alarm is a very low value. MARSAM does not determine higher levels of discrimination in the model, principally because the target sizes considered were not resolvable by FLRs of that generation. This model employs the azimuth resolution given in (40) in conjunction with Johnson's Criteria (see section D) to determine recognition performance.

The capability to provide a moving target indication (MTI) with conventional clutter canceller techniques requires narrow doppler spread of mainbeam clutter. The minimum detectable velocity MDV, can be determined for a typical 4 pole clutter canceller by:

$$MDV = 1.2\ Va \sin \alpha_s / a \qquad (44)$$

where the additional terms are:

Va	=	Aircraft velocity
α_s	=	Scan angle

Matched filter processing may be employed in range-gated MTI radars to sharpen the filter voltage response roll-off. The performance simulated in the MARSAM program is representative of a 4 pole analog systems characterized by a fast Fourier recursive filter (about 12 db/octave slope). The slope can be modified by changing an input notated as an "MF factor." Current digital technology permits the integration of many pulses over the target's doppler history to achieve from 16-32 sub-clutter visibility. The MF factor was set equal to 24 db/octave for multi-mode radars such as the Advanced Tactical Radar based on discussions with engineers at AFAL/RW and ASD/EN.

B. SYNTHETIC APERTURE RADARS

The operational range of synthetic aperture radar is determined by the same physical laws as stated in Equations (39) and (40). Resolution performance is, however, essentially independent of range. The beam of a synthetic aperture radar must be directed at an angle off the direction of aircraft flight. Thus, a doppler phase history can be collected for each imaged target, the length of which increases with increasing range. Figure 9 depicts the essential technology concept. The determination of ground resolution Dgx and Dgy is taken from the MARSAM II approach. The equivalent linear measure of resolution is taken as the geometric mean of the along-track and cross-track resolution.

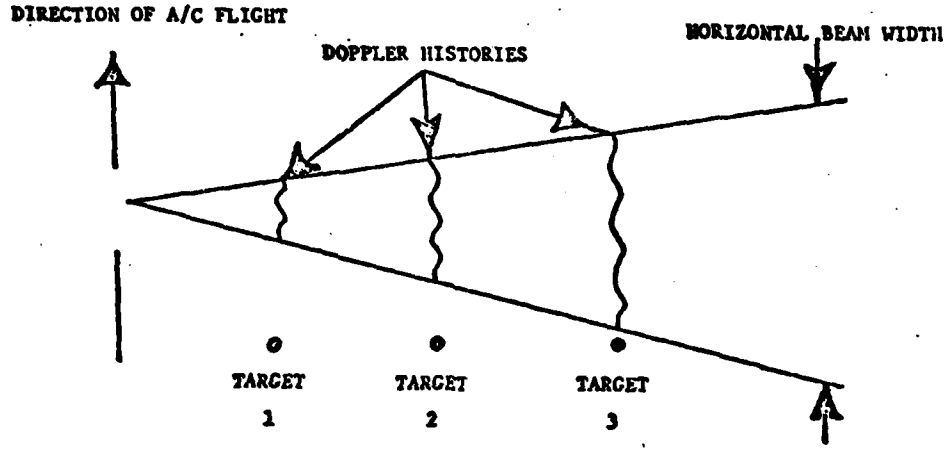

Figure 9. Synthetic Aperture Radar Technology

Since the velocity of the aircraft is known, the collected histories may be processed (integrated) so that each target may be correlated on a ground map which is constant in scale over the imaged area.

Until recently the electrical doppler phase histories were recorded in flight on photographic film. Processing was accomplished on the ground using holographic techniques. This was a time-consuming and cumbersome procedure. Systems now under development may be processed inflight digitally, although the computer size practical in tactical aircraft permits only a small ground area to be displayed in real time. Further developments permit the SAR beam to be directed at angles from 20° to 120° off the axis of the flight path using Cassegrain antenna designs.

The MARSAM model was modified to account for this variable, viewing geometry and real-time cockpit display. Figure 10 depicts the unique geometry of this situation. The correlation process produces a map which moves at the speed of the aircraft at all points of the imaged area. The target size is likewise independent of range to the aircraft. Assuming that the full width of the display is used, the ratio of target area to search area on the display is:

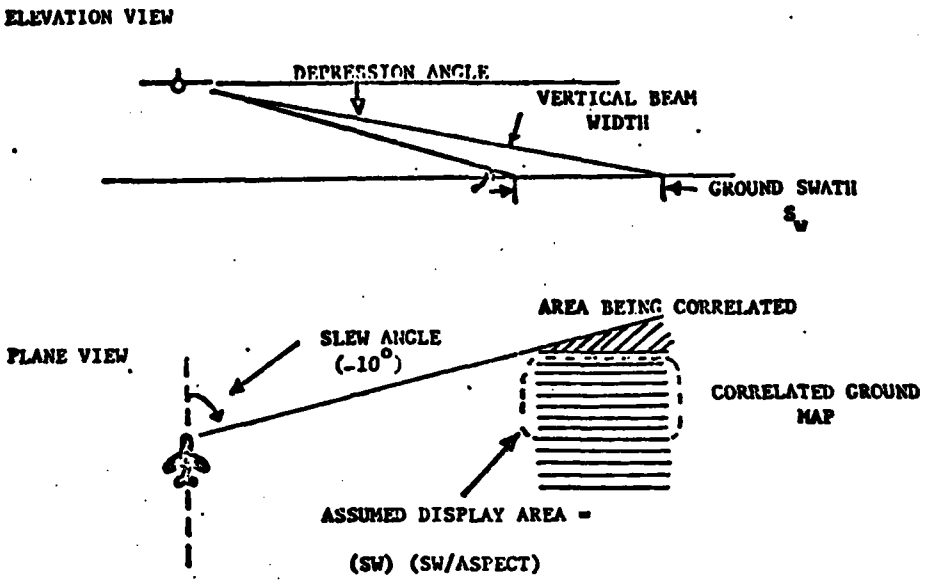

Figure 10. SAR Cockpit Display Geometry

$$a_t / a_s = D_{gx} D_{gy} / Sw \ (Sw / ASPECT) \quad (45)$$

where:

Sw	=	Ground swath
ASPECT	=	The ratio of the vertical to horizontal dimensions of the cockpit display

(U) The time in view, t_f, is therefore:

$$t_f = (Sw / ASPECT) / Va \quad (46)$$

where:

V_a	=	Velocity of the aircraft

These terms are used in the search model developed in Section C.

C. TARGET SIGNATURE CONSIDERATIONS

The return produced by a tactical target illuminated in the microwave region is dependent on the geometry of the viewing and the frequency of the illuminator. Recent studies (reference 13) have shown with respect to the latter that a good (2 dbsm) analytic approximation to the frequency dependency is:

$$\sigma_{50} = S\, f^{.3} \tag{47}$$

where:

σ_{50}	=	Median RCS in square meters
S	=	Median RCS at the radar frequency
f	=	Frequency of the radar in Ghz

(U) Data measurements for a combat tank equivalent to the T-54 have established that S=11.7; therefore, for an X-band

$$\sigma_{50} = 11.7\ (10)^{.3} = 23.3 = 13.7\ db_{sm} \tag{48}$$

which agrees well with field measurements by BRL and others. These data are for a horizontally polarized transmitter and receiver. However, vertical polarization has negligible impact (less than 1 dbsm) on the RCS in the frequencies of interest. The RCS increases approximately 1 db_{sm} for every 15 degrees of depression and decreases with aspect such that at 45° a 5 db_{sm} reduction is observed for tactically-sized targets. These approximations were used in the model to determine the performance of the radar systems. It is felt that the flexibility gained in this completely analytic approach outweighed the possible errors of second order.

RCS data for other targets may be obtained from the MARSAM data base if analytic representations are not available. Background signature data is not as sensitive to wavelength as is the target RCS. The normalized radar cross-section data used in the MARSAM data base, therefore, provides sufficient accuracy. The data for nominal X-band (3.2 cm) and Ku-band (1.8 cm) wavelengths are reproduced in Table 3 for cases of interest.

TABLE 3. MARSAM BACKGROUND SIGNATURE DATA

MARSAM ID CODE NO.	BACKGROUND TYPE	DEPRESSION ANGLE	NORMALIZED RADAR CROSS-SECTION	
			X-BAND	KU-BAND
		ø (deg)	(db)	(db)
1 A-C	ASPHALT	5	-43	-38
		40	-29	-25
		75	-25	-20
2 A-C	CONCRETE ROAD	5	-48	-44
		40	-26	-31
		75	-32	-22
3 A-C	DIRT ROAD	5	-37	-24
		40	-25	-17
		75	-18	-10
11 A-C	DRY MEADOW	5	-24	-22
		80	-21	-19
		75	-17	-16
13 A-C	SNOW	5	-25	-30
		80	-19	-23
		75	-13	-12
14 A-C	WATER, SEA STATE 0	5	-40	-39
		40	-39	-35
		75	-15	-14

V. ATMOSPHERIC EFFECTS

A. GENERAL

The transmittance of an electromagnetic signal through the atmosphere is dependent on the signal wavelength and the physical profile of the signal path.

Opaque regions occur at those wavelengths which are strongly attenuated due to the presence of molecules, aerosols, precipitation, etc., in the intervening medium. Some wavelengths are not as strongly attenuated; therefore, there occurs, within portions of the spectrum, transparent "windows" as may be seen in Figure 11.

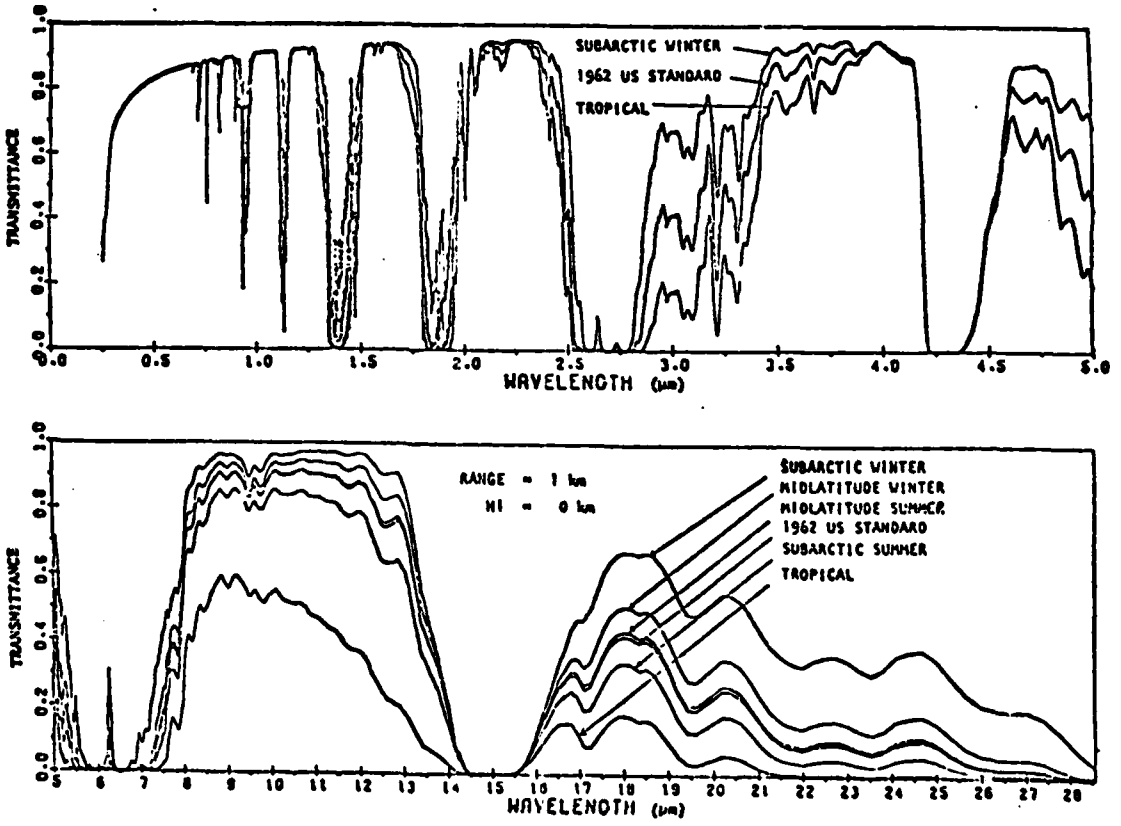

Figure 11. Atmospheric Transmittance for a Path at Sea Level or Six Model Atmospheres

The data plotted in the figure are the results of a computer model developed by the Air Force Cambridge Research Laboratory (AFCRL) entitled *LOWTRAN II*. The model results compare favorably with empirical measurements made by Taylor and Yates [1966] and others.

There are rather large windows in the visible light/near IR region (.4-1.0 μm), and in two areas of the longer wave IR — 3-5 μm and 8-12 μm. These are current areas exploited for tactical EO sensors. The figure depicts six model atmospheres which differ principally in the amount of vaporized water per unit volume (or absolute humidity). Since the effects of absorption by the water vapor continuum are more critical for the longer wavelengths, the selection of the model atmosphere has great impact on the results obtained for FLIR models. Since meteorological visibilities are by definition specified in the visible light region, the transmittance in that region will be the same for all atmospheres. The US Standard Atmosphere is used in this model to estimate the extinction due to scattering along the sensor target path.

B. VISIBLE LIGHT REGION

Two alternatives are offered for determining atmospheric effects in the visible light region; (1) an analytic approach based on the work by Duntley, and (2) an empirical approach using data supplied by AFCRL or any other data which may be available to the user.

1. Analytic Approximation

The model employs the Duntley sky/ground ratio approach to account for the effects of path radiance in the visible light region. For reasonable attack profiles (i.e., with the sun abeam or behind the attacking aircraft) it can be shown that the sun/target/sensor geometry does not have a significant impact on the results. Duntley has developed a formulation for estimating the apparent contrast, C_a, which is appropriate in such circumstances, viz:

$$C_a = C_0 / [1+K(1-T_{at})/T_{at}] \quad (49)$$

where:

C_o	=	Inherent Contrast
T_{at}	=	Beam Transmittance
K	=	The Sky/Ground Ratio

The sky/ground ratio may be measured directly with a photometer, or, according to Middleton, it may be estimated with reasonable accuracy through the relationship:

$$K = Q / \rho_{te} \quad (50)$$

where:

ρ_{te}	=	The reflectance of the general background (not necessarily the background in the immediate target area).
Q	=	A factor to account for the impact of clouds on the overall scene illuminance. Q varies from 1 (solid overcast) to .2 (clear).

A table of background reflectance values for use in Equation (50) is given in Table 4.

TABLE 4. BACKGROUND REFLECTANCE VALUES

TYPE OF BACKGROUND	REFLECTANCE VALUE (ALBEDO)
OPEN SEA	0.50
SNOW	0.77
DESERT	0.25
FOREST	0.10
EARTH	0.03
DRY MEADOW	0.08

Beam transmittance is defined as:

$$T_{at} = \exp(-\sigma R) \tag{51}$$

where:

R = Slant range to the target in feet

σ = Extinction coefficient (FT^{-1})

A formulation for beam transmittance in terms of meteorological visibility can be obtained if the atmosphere is uniform. The meteorological visibility is defined as the range at which the contrast of a dark object against the sky is reduced to 2 percent. Meteorological visibility is measured from the observer to the horizon sky. Therefore, for a path to the horizon:

$$T_{at} = \exp[-(3.91\ R)/V_m)\ (\lambda/.55)^{-1}] \tag{52}$$

where

R = Range to the target

V_m = Meteorological visibility

λ = Wavelength in which measured

For any visual plane other than the ground plane, use of the meteorological visibility in the exponent will estimate T_{at} pessimistically. This will result because there are fewer molecular and aerosol components of the atmosphere with increasing altitude, and correspondingly less extinction of the signature because of scattering and absorption of the radiant energy. Assuming a uniformly decreasing density with altitude and a molecular and aerosol cross-section equal to the US Standard Atmosphere, the ratio of meteorological visibility to slant range visibility for an air-to-ground (or ground-to-air) path from any altitude may be estimated using Figure 12. An analytic approximation to this curve which gives slant range visibility, V_s, directly and is good for altitudes up to about 50,000 feet is:

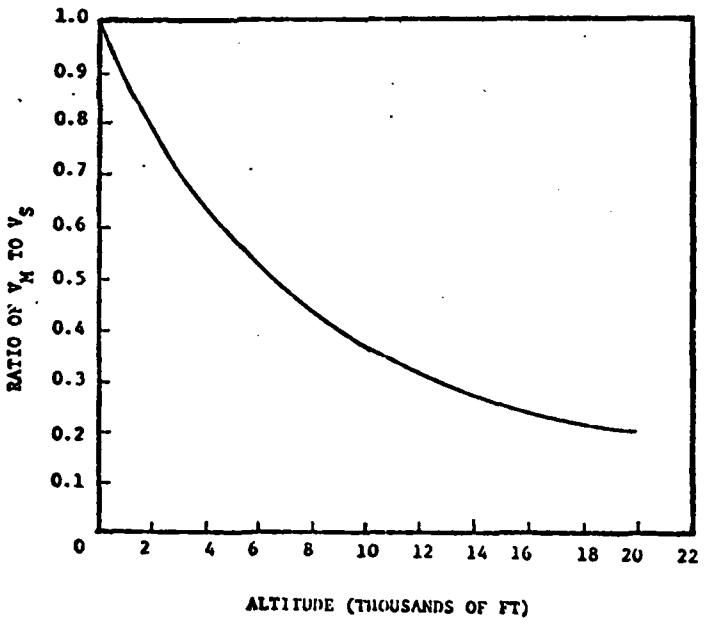

Source: RCA HB (US Std Atmosphere)

Figure 12. Ratio of V_M to V_S Versus Altitude

$$V_s = V_m / [.44/(A + 1.2) + .56 \exp(-.08A) + .073] \quad (53)$$

where:

V_m = Meteorological visibility (nm) measured in ground plane

A = Altitude in thousands of feet

Beam transmittance for .55μm (visible light) is then:

$$T_{at} = \exp ((3.91 R) / (6076 V_s)) \quad (54)$$

The chart in Section A, demonstrating beam transmittance approximation based on the US Standard Atmosphere, is sufficiently accurate for any geographical location within the visible light region. The differences between model atmospheres lie principally in the amounts of H_2O continuum*. The extinction due to H_2O absorption in the visible light region is negligible, therefore, no significant differences in beam transmittance values are obtained with other models.

2. Empirical Data

The model has been modified to accept empirical data on atmosphere when available. AFCRL has supplied data taken from a set of representative flight profiles over southwestern Germany for comparative purposes. The weather during the data collection was good by Central European standards; scattered clouds and a nine nautical mile meteorological visibility. There was a thin haze layer prevalent at about 1000 feet AGL.

To understand the employment of the AFCRL data on this model,

* Model atmospheres in general use are: Subartic Winter, Mid-latitude Winter, Mid-latitude Summer, 1962 US Standard, Subartic Summer, and Tropical.

one must derive the contrast transmission term using the expression for contrast ratio (C_0) as defined by manufacturers of EO systems:

$$C_0 = (B_{max_0} - B_{min_0}) / B_{max_0} \tag{55}$$

where the notations max and min establish the greater and lesser brightness of the target and its background at range zero. Now at range r, the contrast ratio C_r becomes:

$$C_r = \frac{B_{max_0} T_{at} + P - (B_{min_0} T_{at} + P)}{B_{max_0} T_{at} + P} \tag{56}$$

where:

P = Path radiance

Defining contrast transmission, T_c, as:

$$T_c = C_r / C_o \tag{57}$$

The terms $(B_{max_0} - B_{min_0})$ cancel and with a little algebraic manipulation:

$$T_c = 1 / [1 + P/(B_{max_0} T_{at})] \tag{58}$$

The brightness of any object at range zero, B_0, is:

$$B_0 = \rho_d H / \pi \tag{59}$$

where:

ρ_d = Directional reflectivity

H = Illuminance

$$T_c = 1 / [1 + \pi P / \rho_{dmax} H T_{at}] \tag{60}$$

AFCRL had reduced the data from two selected profiles such that the terms in the denominator, $\frac{\pi P}{H T_{at}}$, is a dimensionless entity R*. Then:

$$T_c = 1 / [1 + R^* / \rho_{dmax}] \quad (61)$$

ρ_{dmax} is obtained by multiplying the maximum of either the target or immediate background albedo by the directional reflectivity factor, F, for the zenith angle determined by the slant range - altitude geometry. Figures 13 and 14 present values for R* for flight profiles directly into and abeam of the sun. Notice the intersection of the 1000' and 1500' altitude curves caused by the existence of the haze layer.

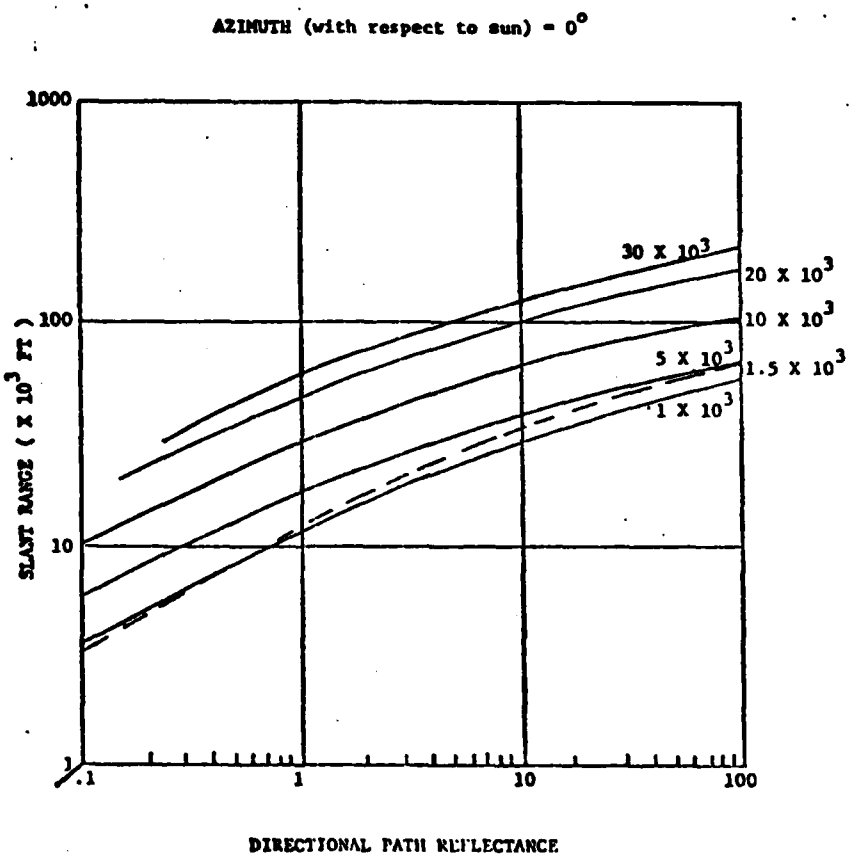

Figure 13. Directional Reflectance vs Slant Range for Selected Altitudes

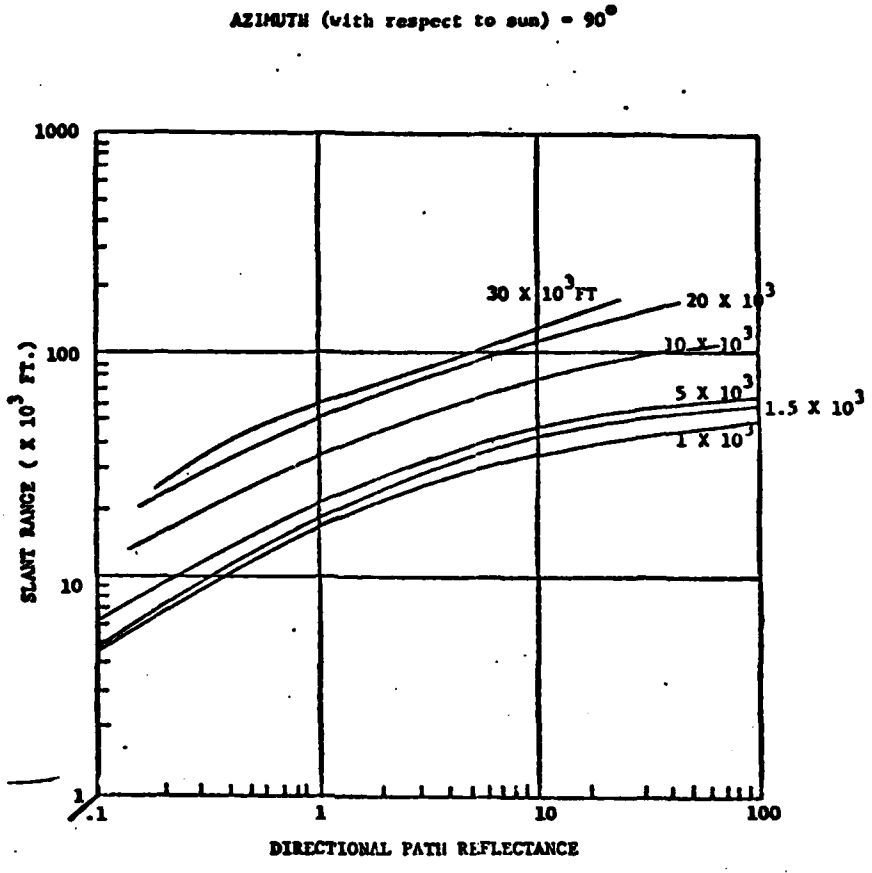

Figure 14. Directional Reflectance vs Slant Range for Selected Altitude

One further data item is needed to use the AFCRL data. The reflectance of all substances is directional to some extent. This directivity is not an important factor for very diffuse reflectors or for near-nadir geometry. However, for man-made objects such as asphalt roads, or metal surfaces, this directivity must be accounted for.

All existing models examined by the author have ignored the specular effects and used albedo values (average over the hemisphere).

Figure 15 presents an average of several man-made objects having low albedos; i.e., the order of 0.10. Notice that there is a decrease in directional reflectance for sun azimuth of 90 degrees until a zenith angle of about 150 degrees is reached. Directional reflectance for a mean azimuth of 0 degree increases monotonically with decreasing sun angle.

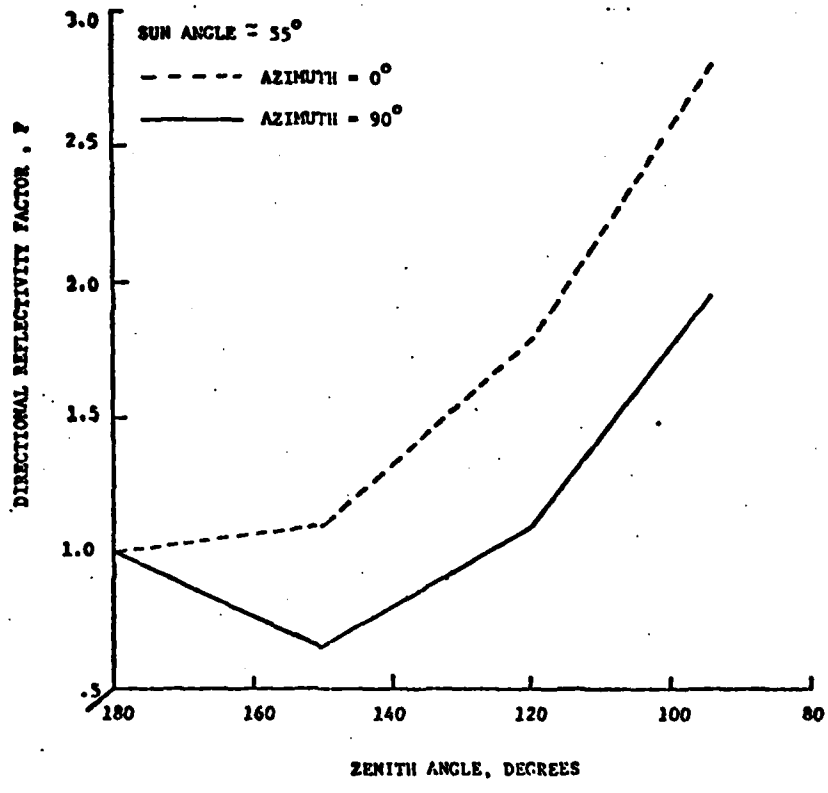

Figure 15. Assumed Directional Reflectivity Factor

C. INFRARED REGION

The model is currently developed to estimate extinction in the 8-13 μm region from the reported meteorological visibility, temperature and relative humidity. The methodology follows a series of curve fits developed by Miller (reference 12) and based on transmittance data reported by Altshuler. The normalized distribution of aerosol particles and water vapor with altitude are taken from the work of McClatchey (reference 15), and are therefore consistent with the LOWTRAN model atmospheres.

(U) The total transmittance of IR energy over a given slant path T_a, is:

$$T_a = T_{pwv}\, T_{ae} \tag{62}$$

where:

T_{pwv}	=	Transmittance due to absorption by precipitable water vapor (PWV)
T_{ae}	=	Transmittance due to aerosal scattering

Figure 16 depicts the transmittance of energy in the 8-13 μm region for a path having a uniform PWV distribution as determined by Altshuler. A reasonable fit to this curve is obtained with:

$$T_{pwv} = \exp(-.017\, w) \tag{63}$$

where: w = pwv in mm/kilofeet

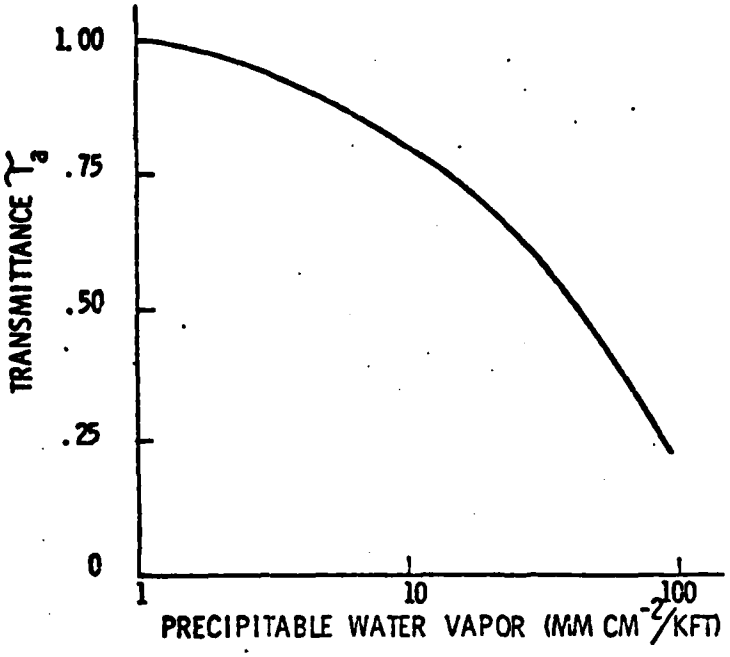

Figure 16. Precipitable Water Vapor Absorption (8-13μm) (Altshuler)

The amount of precipitable water vapor at sea level, W_o, can be estimated from the temperature and relative humidity by:

$$W_o = 1.432\ H_r \exp(-.0652)\ (T_B - 273) \tag{64}$$

where:

H_r = relative humidity

T_B = temperature of the background (°K), $263 \le T_B \le 313$

It can be demonstrated that the ratio of precipitable water vapor at altitude h to that at sea level W/Wo is essentially the same for all model atmospheres and can be approximated by:

$$W/W_0 = \exp(-.13\ h) \tag{65}$$

where: h = altitude in kilofeet

The ratio of the aerosol particle density at altitude h to the sea level value, P/Po, can be similarly shown to be approximately:

$$P/P_0 = \exp (-.28\ h) \tag{66}$$

Miller develops the above terms in a convenient analytic relationship using a mean value for T_{ae} of .998 in the 8-13 μm region for a standard 23 km. meteorological visibility day. The resulting expression for equation (62) is:

$$T_a = \exp (-G\ R) \tag{67}$$

where: R = The slant range to the target in kilofeet

$$G = \frac{.278\ D_2 + .017\ W_o\ D_1}{V_m}$$

and V_m = meteorological visibility in kilofeet

$$D_1 = \frac{1}{.13\ h} [\ 1 - \exp (-.13\ h)\ ] \tag{68}$$

$$D_2 = \frac{1}{.28\ h} [\ 1 - \exp(-.28\ h)\ ] \tag{69}$$

where h is in kilofeet.

The above formulation was recently compared with more rigorous approaches by a group of AFIT students for a graduate group exercise. The exponential assumptions were found to give good results up to about 20,000' AGL. The disparaties in model results were found to be greater at the lower relative humidity conditions, which are not of particular interest in the selected scenario. More accuracy may be obtained with higher order fits to the empirical data presented above.

D. MICROWAVE REGION

Rain and clouds are the only significant attenuators of electromagnetic waves in the X and K_u bands. The model employs a slant path attenuation scheme developed in USAFE TAC Report 7599 for the Central European environment. That report contains extensive data on the frequency and extent of meteorological phenomena which affect radar performance by season and time of day. Limited portions of the data were selected for application in the model.

The data points utilized are determined by two parameters: the season and the cumulative attenuation sum (CAS). The CAS value specifies the attenuation case to be considered, its value being the sum of all cases with attenuation less than that considered.

Attenuation along a specific path may be calculated in the no precipitation case by:

$$A_{db} = K_\lambda L_{wc} X \tag{70}$$

where:

L_{wc} = Liquid water content (gm/m^3)

X = Slant range through clouds (km)

K_λ = Wavelength dependent constant

= .20 for K_u-band

= .06 for X-band

The slant range path is determined in the model from the geometry of the approach with inputs of the cloud layer vertical profile. The average

liquid water content is then scaled according to the meteorological extent of the clouds through use of the CAS value.

Rain attentation is performed similarly to the no precipitation case. Rain requires a solid overcast so the probabilities for cloud cover and precipitation are dependent allowing the use of one CAS term. The precipitation is assumed to commence at the lower boundry of the cloud layer and to be homogeneous to ground level. The rain attenuation rates used in the report are plotted in Figure 17 The resolution advantages of the shorter wavelength K_u-band radar may be offset by the higher attenuation under adverse weather conditions.

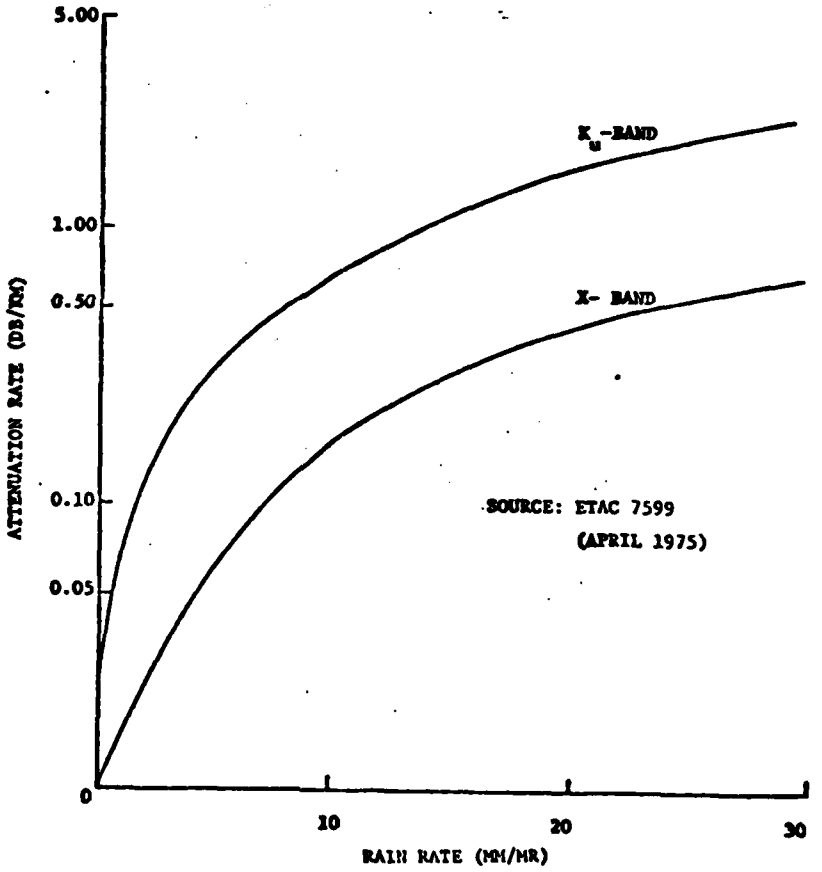

Figure 17. One Way Transmission of Radar Energy

REFERENCES

1. "Image Interpretation Handbook", Vol II, AFM 200-5, 1967, CONFIDENTIAL.

2. "Advanced Tactical Fighter Acquisition and Weapon Delivery Study", Final Report for Contract F33615-74-C-4052, McDonnell Douglas Corp., St. Louis, Missouri, October 1974, SECRET.

3. Greening, C. P., "Alternative Approaches to Modeling Visual Target Acquisition" NWC Working Paper, September 1974.

4. Bailey, H. H., "Target Detection Through Visual Recognition: A Quantitative Model", Report RM-6158-PR, The RAND Corp., February 1979.

5 Hilgendorf, R. L., "Enhancement of Target/Background Contrasts in Search and Rescue Applications", AMRL-TR-72-4, 1972.

6. Johnson, J., "Analysis of Image Forming Systems", Proceedings of Image Intensifier Symposium, US Army Corps of Army Engineers, Ft. Belvoir, VA, October 1958.

7. Rosell, F. A. and Wilson, R. H., "Performance Synthesis of Electro-Optical Sensors", AFAL-TR-74-104, Westinghouse Corp., Baltimore, MD, April 1974.

8. Lippiatt, T. F., "TV Sensor Aided Target Acquisition Model for RPVs", R-1437-PR (Draft), The RAND Corp., February 1975.

9. Hammill, H. B., et al, "A Modified Model for Visual Detection", Interim Technical Report prepared for Contract F33615-68-C-1319, Cornell Aeronautical Laboratory, Inc., 1968.

10. Sendall, R. L., and Rosell, F. A., "E/O Sensor Performance Analysis and Synthesis", Final Report for Contract F33615-70-C-1682, Air Force Avionics Laboratory, WPAFB, Ohio, April 1973.

11. Biberman, L. C., "The Methodology of the Analysis" Working Paper, prepared for IDA/WSEG SEEK VAL Study effort, 25 February 1975.

12. Miller, Phillip C., "A Static Performance Prediction Airborne Model for an Imaging IR System", Paper presented at the NAECON Symposium, Dayton, Ohio, June 1975.

13. "Multiple Airborne Reconnaissance Sensor Assessment Model" (MARSAM II), Honeywell Technical Report, ASD-TR-68-3, February 1968.

14. Mirmak, E. V., "Tank Radar Cross-Section Data" AFAL-TM-75-10-AFAL/RWA-2, 1975, SECRET.

15. McClatchey, R. A., "Optical Properties of the Atmosphere" AFCRL-72-0497, Air Force Cambridge Research Laboratories, 24 August 1972.

16. RF-15, Advanced Tactical Reconnaissance Aircraft Study, Final Report, Vol 1, 2 and 3, 28 September 1973, McDonnell Aircraft Company, SECRET.